

# Magnetic field-enhanced spin filtering in rare-earth mononitride tunnel junctions

P. K. Muduli<sup>1</sup>, X. L. Wang<sup>2</sup>, J. H. Zhao<sup>2</sup>, Mark G. Blamire<sup>1</sup>

<sup>1</sup>*Department of Materials Science and Metallurgy, University of Cambridge,  
27 Charles Babbage Road, Cambridge CB3 0FS, United Kingdom\* and*

<sup>2</sup>*State Key Laboratory of Superlattices and Microstructures,  
Institute of Semiconductors, Chinese Academy of Sciences, Beijing 100083, China*

Spin filter tunnel junctions are based on selective tunneling of up and down spin electrons controlled through exchange splitting of the band structure of a ferromagnetic insulator. Therefore, spin filter efficiency can be tuned by adjusting exchange strength of the tunnel barrier. We have observed that magnetic field and bias voltage (current) can be used to regulate exchange strength and consequently spin-filter efficiency in tunnel junctions with ferromagnetic DyN and GdN tunnel barrier. In tunnel junctions with DyN barrier we obtained  $\sim 37\%$  spin polarization of tunneling electrons at 11 K due to a small exchange splitting ( $E_{ex}$ )  $\approx 5.6$  meV of the barrier height ( $\Phi_0$ )  $\approx 60$  meV. Huge spin-filter efficiency  $\sim 97\%$  was found for tunnel junctions with GdN barrier due to larger  $E_{ex} \approx 47$  meV. In the presence of an applied magnetic field, barrier height can further split due to magnetic field dependent exchange splitting  $E_{ex}(H)$ . The spin filter efficiency in DyN tunnel junctions can be increased up to  $\sim 87\%$  with magnetic field. Electric and magnetic field tuned spin-filter efficiency of these tunnel junctions gives opportunity for practical application of these devices with additional functionality.

## I. INTRODUCTION

The creation, injection and transport of spin-polarized current are the three basic steps in all spintronics devices. Instead of relying on conventional ferromagnets for creation, fully spin polarized currents can also be generated using spin-filter tunneling of electrons through a ferromagnetic tunnel barrier. The spin-up and spin-down electrons of a non-magnetic electrode passing through a spin-filter tunnel barrier can be filtered due to the difference in tunnel barrier heights for the two spin channels<sup>1,2</sup>. The difference in barrier height appears due to exchange splitting of the band structure, which leads to the conduction band minima and valance band maxima at different energies for majority and minority spin electrons. Spin filter tunnel barrier can also solve impedance mismatch problem with semiconducting counter electrodes facilitating in spin injection from even a nonmagnetic metal into a semiconductor<sup>3</sup>. Many ferromagnetic insulators have been tested for their spin filtering property: the Eu chalcogenides including EuS<sup>4,5</sup>, EuSe<sup>6</sup>, EuO<sup>7</sup>, etc. have shown high spin filtering efficiency; oxides like CoFe<sub>2</sub>O<sub>4</sub><sup>8,9</sup>, NiFe<sub>2</sub>O<sub>4</sub><sup>10</sup>, BiMnO<sub>3</sub><sup>11</sup>, NiMn<sub>2</sub>O<sub>4</sub><sup>12</sup>, CoCr<sub>2</sub>O<sub>4</sub><sup>13</sup> and Sm<sub>0.75</sub>Sr<sub>0.25</sub>MnO<sub>3</sub><sup>14</sup>, etc. have also received a lot of attention due to their higher Curie temperature, but to date, the spin filter efficiencies have been low.

Many of the rare earth mono nitrides (REN) are magnetic semiconductors in which magnetic and electronic properties are strongly coupled<sup>15,16</sup>. Magnetism in REN is very complex and not yet fully understood; some of these materials display a peculiar type of forced ferromagnetism called metamagnetism<sup>17</sup>; i.e., they are antiferromagnetic at low magnetic field and forced to be ferromagnetic by applying high magnetic field. Usually RENs undergo a second order magnetic transition from paramagnetic semiconducting behavior to a ferro-

magnetic metallic-like state below the Curie temperature ( $T_{Curie}$ ). As  $4f$  moments in RE atoms are highly localized, the exchange interaction in these compounds is determined by indirect exchange interaction between these localized moments. Most widely studied ferromagnetic REN is GdN which shows the highest  $T_{Curie} \sim 70$  K. Recently, GdN has shown spin filtering effect in NbN-GdN-NbN tunnel junctions<sup>18-20</sup>. This opens up rare earth mono nitrides as another class of spin-filter tunnel barriers. In this paper, we have investigated the spin filtering property of poorly explored DyN and GdN tunnel barriers. DyN is a ferromagnetic semiconductor with  $T_{Curie} \sim 35$  K<sup>21</sup>. DyN has two more  $4f$  electrons than the half-filled GdN and it has the highest saturation magnetization  $\sim 10\mu_B/\text{Dy}$  among the REN series. Theoretical band structure calculations on DyN show a small indirect  $\Gamma$ -X gap  $\sim 0.34$  eV and a minimum direct gap of  $\sim 1.17$  eV at X<sup>22</sup>. Experimentally DyN has been shown to be a semiconductor with an optical gap of  $\sim 1.2$  eV<sup>23</sup>. Recently, we have made an extensive study of the tunneling property of NbN-DyN-NbN tunnel junctions with different thickness of DyN<sup>21</sup>. We found a crossover from diffusive to tunneling transport as the DyN thickness is made smaller than  $\sim 4$  nm. In this paper, we show that the tunneling properties of DyN and GdN junctions are strongly affected by magnetic field. We demonstrate that splitting of the tunnel barrier height for spin-up and down electron can be further increased with magnetic field. We have explained our data with simple tunneling model of Simmons considering different conductance channel for up-spin and down-spin electrons.

## II. EXPERIMENT

NbN-DyN-NbN and NbN-GdN-NbN trilayer films were deposited on  $5 \times 5 \text{ mm}^2$  Si/SiO<sub>2</sub>(250 nm)/MgO(10 nm)

substrates by reactive DC sputtering. The deposition was done at room temperature with a pressure of  $\sim 1.5$  Pa in an UHV chamber equipped with multiple layer deposition. Top and bottom 50 nm thick superconducting NbN was deposited with 28% Ar-N<sub>2</sub> gas mixture at 100 W sputtering power. Whereas 8% Ar-N<sub>2</sub> gas mixture with lower  $\sim 16$  and  $\sim 20$  W sputtering power was used for DyN and GdN, respectively. The details of deposition condition is described in reference<sup>21</sup>. Trilayers with 2.6 nm GdN and 3 nm DyN barriers were used for tunnel junction fabrication. Eight tunnel junctions of dimension  $7 \times 7 \mu\text{m}^2$  were fabricated on each substrate by optical lithography in conjunction with Ar-ion milling and CF<sub>4</sub> plasma etching. Electrical characterization of the tunnel junctions were done in a four-probe configuration with a closed-cycle He refrigerator from Cryogenic Limited. Although all the junctions behaved in a similar way, for consistency we have shown measurements done on one junction of each type only in this paper. Magnetization measurements were performed in a Quantum Design SQUID magnetometer.

### III. RESULTS

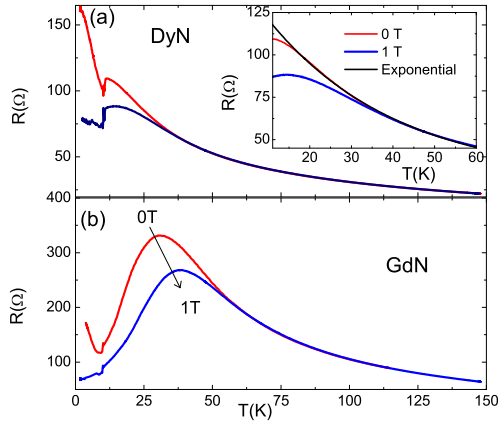


FIG. 1: (Color online) Temperature dependence of resistance of (a) NbN-DyN(3 nm)-NbN and (b) NbN-GdN(2.6 nm)-NbN tunnel junction with zero (red) and 1 T (blue) magnetic field. The measurement was done with a bias current  $I = 1 \mu\text{A}$ .

Figure 1 shows the junction resistance as a function of temperature  $R(T)$  with magnetic field  $\mu_0 H = 0$  and 1 T. Semiconducting behavior can be seen in  $R(T)$  above 11 and 50 K for the DyN and GdN junction, respectively. Evidence for spin filtering is obtained from  $R(T)$  below  $T_{\text{Curie}}$  when exchange splitting of the barrier reduces the barrier height for one spin sign and hence a decrease in the resistance of the junction. Effect of spin filtering can be seen clearly as drop in  $R(T)$  below  $\sim 30$  K in the case of the GdN junction as shown in Fig. 1(b). In the case of the DyN junction the deviation of the experimental  $R(T)$  data below  $\sim 15$  K from the extrapolated exponential fit

above  $\sim 20$  K provides proof that spin filtering is present in these junctions. The spin filtering efficiency can be determined from  $R(T)$  using the method described in the reference<sup>19</sup>. In the low bias limit spin-filter efficiency can be written as,  $P \approx \sqrt{1 - R_r^2}$ , where  $R_r$  is junction resistance relative to the non-magnetic state. For the DyN junction spin filtering efficiency  $P \sim 37\%$  was found at 11 K in zero magnetic field. This is quite small compared to  $P \sim 97\%$  found at 11 K for the GdN tunnel junction. When an in-plane magnetic field is applied we found that the spin filter efficiency increased from  $P \sim 67\%$  at 1 T to  $P \sim 87\%$  at 5 T for the DyN tunnel junction. A small increase of  $P \sim 97\%$  at zero field to  $P \sim 98\%$  at 1 T was found for the GdN junction at the same temperature. The change in slope in the  $R(T)$  ( $dR(T)/dT > 0$  to  $dR(T)/dT < 0$ ) can be used as an indicator of  $T_{\text{Curie}}$ . Fig. 1(b) shows that for the GdN junctions, the  $T_{\text{Curie}}$  is significantly enhanced from 30 to 38 K when 1 T magnetic field was applied. Similar enhancement of  $T_{\text{Curie}}$  can also be seen for the DyN junctions in Fig. 1(a).

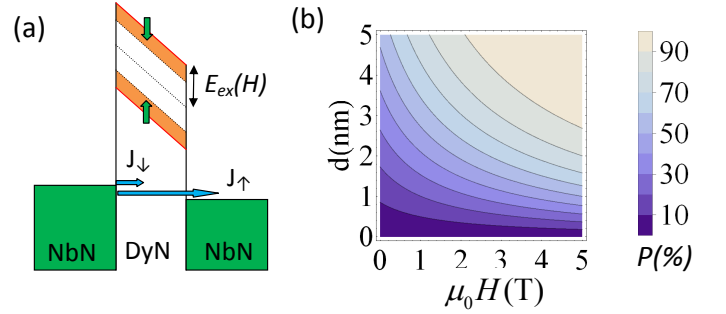


FIG. 2: (Color online) (a) Schematic illustration of the spin filter mechanism in presence of magnetic field. Spin-up and spin-down bands are further split by magnetic field dependent exchange splitting  $E_{\text{ex}}(H)$  (shown in orange color). (b) Expected spin-filter efficiency  $P$  for different thickness  $d$  of the tunnel barrier with magnetic field  $H$ . The spin-filter efficiency was calculated for a barrier with height  $\Phi_0 = 60$  meV and exchange splitting  $E_{\text{ex}}(0) = 5.6$  meV (see text for details).

The tunneling nature of the junctions was confirmed through  $I - V$  measurements at different temperatures. Simmons model<sup>24</sup> was fitted to the  $I - V$  curve above  $T_{\text{Curie}}$  where exchange splitting of the barrier  $E_{\text{ex}} = 0$ . For DyN junction a barrier height  $\Phi_0 = 60$  meV and width  $d = 3.3$  nm were found from the fitting at 50 K (see Supplementary Information<sup>25</sup>). For the GdN junctions Simmons model fitting was done at 100 K and barrier height  $\Phi_0 = 111$  meV and width  $d = 2.8$  nm were found from the fitting. The  $I - V$  and  $dI/dV - V$  measurement of both the DyN and GdN junctions at 4.2 K showed clear superconducting gap structure. This confirms that the electrical transport in our device is dominated by tunneling process.

The mechanism of spin-filtering in presence of a magnetic field can be understood with a tunneling model as shown in Fig. 2(a). Below  $T_{\text{Curie}}$ , the conduc-

tion band is split by the ferromagnetic exchange interaction leading to a lower barrier height  $\Phi_{\uparrow} = \Phi_0 - E_{ex}$  for up-spin and higher  $\Phi_{\downarrow} = \Phi_0 + E_{ex}$  for down-spin electrons. The spin filtering efficiency is usually given by,  $P = \frac{J_{\uparrow} - J_{\downarrow}}{J_{\uparrow} + J_{\downarrow}}$ , where  $J_{\uparrow}$  and  $J_{\downarrow}$  are spin-up and spin-down current density, respectively<sup>7</sup>. As per the Wentzel-Kramers-Brillouin (WKB) approximation the tunneling current density for each spin sign exponentially depends on the relevant barrier height  $\Phi_{\uparrow}$  (or  $\Phi_{\downarrow}$ ) and can be written as  $J_{\uparrow(\downarrow)} \propto \exp(-\frac{2d}{\hbar} \sqrt{2m\Phi_{\uparrow(\downarrow)}})$ ; where  $d$  is the thickness of the tunnel barrier and  $m$  is the electron mass. In the presence of a magnetic field the barrier height can further change due to magnetic field dependence of exchange splitting  $E_{ex}(H)$ . The additional spin splitting of the tunnel barrier due to magnetic field is shown in Fig. 2(a). Considering magnetic field dependency on barrier height, the spin filter efficiency at very low applied bias voltage ( $V \rightarrow 0$ ) can be written as;

$$P = \frac{e^{-\frac{2d}{\hbar} \sqrt{2m[\Phi_0 - E_{ex}(H)]}} - e^{-\frac{2d}{\hbar} \sqrt{2m[\Phi_0 + E_{ex}(H)]}}}{e^{-\frac{2d}{\hbar} \sqrt{2m[\Phi_0 - E_{ex}(H)]}} + e^{-\frac{2d}{\hbar} \sqrt{2m[\Phi_0 + E_{ex}(H)]}}} \quad (1)$$

The exchange splitting  $E_{ex}(H)$  can be calculated with a known value of the spin-filter efficiency using Eq. [1]. At 11 K using  $P \sim 37\%$  for the DyN tunnel junction we found  $E_{ex}(0) \approx 5.6$  meV for  $H = 0$  T. Similar calculations gave  $E_{ex}(0) \approx 47$  meV at 11 K for the GdN tunnel junctions. The spin-filter efficiency is usually determined by the ratio  $E_{ex}/\Phi_0$  which is only  $\sim 0.09$  for DyN tunnel junction. In GdN tunnel junction  $E_{ex}/\Phi_0 \sim 0.42$ . For comparison, in EuO spin-filter junctions  $E_{ex}/\Phi_0 \sim 0.3$  which leads to a very high spin-filter efficiency  $\sim 98\%$ <sup>7</sup>. Figure 2(b) shows the calculated spin-filter efficiency using Eq. [1] in the magnetic field range  $\mu_0 H = 0$  to 1 T for tunnel barrier in the thickness range 1 to 5 nm. The magnetic field dependence of exchange splitting was assumed to be,  $E_{ex}(H) = E_{ex}(0) + \alpha_s H$  for the calculation of  $P$ . Here  $\alpha_s$  is a temperature dependent constant. Justification for such assumption is given in the discussion section later on. For the calculation  $\Phi_0 = 60$  meV,  $E_{ex} = 5.6$  meV, and  $\alpha_s = 0.004$  was used. Clearly very high spin-filter efficiency up to  $\sim 100\%$  can be obtained in thicker tunnel junctions with smaller magnetic field. Therefore, magnetic field can be used to tune spin-filter efficiency in our tunnel junctions.

Figure 3(a) and (b) show normalized junction resistance  $R_N(H) (= R_J(H)/R_J(0))$  at different temperatures for the DyN and GdN tunnel junction, respectively. At 100 K negligibly small change in  $R_N(H)$  with magnetic field was found for both DyN and GdN tunnel junction. As temperature is decreased  $R_N(H)$  is found to decrease rapidly with magnetic field. A much larger decrease  $\sim 70\%$  was found for the GdN junctions compared to  $\sim 45\%$  in the DyN junction at the same temperature (20 K). The  $R_N(H)$  showed nonlinear dependence with magnetic field which becomes prominent as temperature is decreased. As the junctions were cooled down below

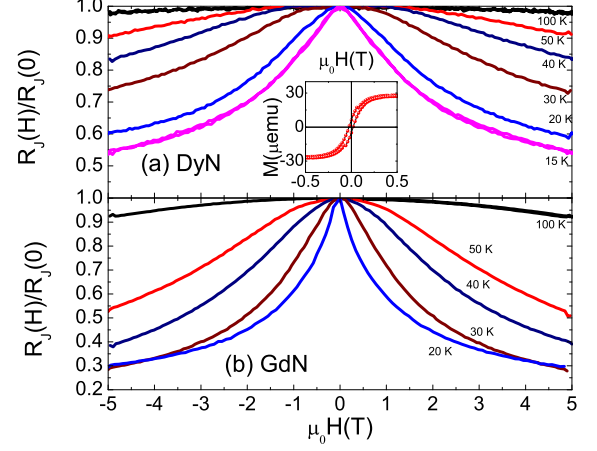


FIG. 3: (Color online) Magnetic field dependence of normalized junction resistance  $R_N(H) (= R_J(H)/R_J(0))$  of the (a) NbN - DyN(3 nm)- NbN and (b) NbN-GdN(2.6 nm)-NbN tunnel junction in the temperature range 15-100 K. Inset in Fig. 1(a) shows magnetization  $M(H)$  measurement at 13 K of a NbN-DyN(3 nm)-NbN trilayer film deposited at the same time.

$T_{Curie}$  the magnetization of the tunnel barrier increases along with increase in spin-filter efficiency. Therefore, the rapid decrease of  $R_N(H)$  along with increase in non-linearity at lower temperature can be understood by considering the magnetic field dependence of barrier heights  $\Phi_{\uparrow(\downarrow)}$ . Field dependence of magnetization of the NbN-DyN(3 nm)-NbN trilayer film measured at 13 K is shown in the inset of Fig. 3. The film was deposited at the same time as the trilayer from which tunnel junction is fabricated.

We also measured the magnetic field dependence of the junction resistance with different bias current. Fig. 4(a) and (b) shows the field dependence of  $R_N(H)$  measured at 11 K with bias current  $I = 10 \mu A$  to 1 mA. The measurements were done in a constant current mode. We also found similar results with measurements done in a constant voltage mode (see Supplementary material). For the DyN junction at low bias current  $\sim 10 \mu A$  we found  $\sim 45\%$  decrease in  $R_N(H)$  with a magnetic field of 5 T. Larger  $\sim 56\%$  decrease in  $R_N(H)$  was found for the GdN junction. As bias current was increased to  $\sim 1$  mA the change in  $R_N(H)$  was found to reduce significantly along with suppression of nonlinearity. The DyN junctions showed much stronger bias current dependence compared to GdN junctions.

#### IV. DISCUSSION

In spin-filter tunnel junctions difference in barrier height for spin-up and down electrons appear because of the exchange splitting of the conduction band of the

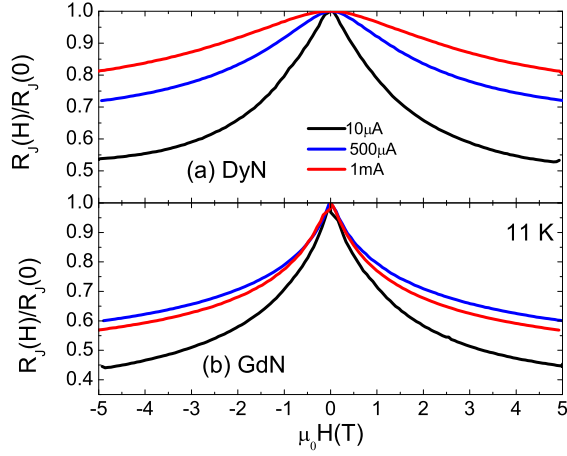


FIG. 4: (Color online) Magnetic field dependence of normalized junction resistance  $R_N(H) (= R_J(H)/R_J(0))$  of the (a) NbN - DyN(3 nm)- NbN and (b) NbN-GdN(2.6 nm)-NbN tunnel junction at 11 K with different bias current. Measurement was done in a constant current mode with different current values.

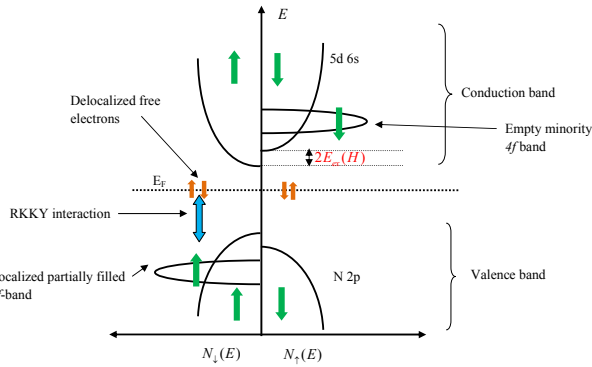


FIG. 5: (Color online) Schematic of a simplified band diagram of REN.<sup>22,26,27</sup>

ferromagnetic semiconductor below  $T_{Curie}$ . Therefore, a detail understanding of the temperature and magnetic field dependence of exchange splitting can be obtained from the band structure<sup>28,29</sup>. Fig. 5 shows schematic of a simplified band diagram of REN (more accurately for GdN and DyN). In REN the valence band is usually formed from N 2p band which is hybridized with RE 5d (6s) bands. While the conduction band comprises RE 5d and 6s bands which is also hybridized with N 2p bands. The majority RE 4f spin-up band is partially filled and lies below the valence band maximum. The empty minority spin-down 4f band lies above the conduction band minimum. As 4f bands are highly localized with no direct orbital overlap, the  $f-f$  band interaction between neighboring RE atoms is very weak. The magnetism in REN arises due to many competing direct and indirect exchange interactions between 4f bands. Be-

sides carrier mediated Ruderman-Kittel-Kasuya-Yoshida (RKKY) type exchange interaction is also proposed to exist in REN<sup>30</sup>. The delocalized free electrons close to Fermi level can mediate such interaction. The magnetism in REN is quite complex compared to transition metal ferromagnets where  $d$  electrons are more itinerant in nature. Magnetism in REN can be appropriately described by Heisenberg type Hamiltonian

$$H = - \sum_{i,j} J_{ij} S_i S_j, \quad (2)$$

where  $J_{ij}$  are exchange coupling constant between the localized spin on the site  $i$  and  $j$ . In a mean field approximation the Curie temperature can be written as<sup>31,32</sup>

$$k_B T_{Curie} = (2/3) S(S+1) \sum_{m=1}^N z_m J_m, \quad (3)$$

where  $z_m$  is the number of nearest neighbor and  $J_m$  is corresponding exchange coupling constant. Here  $S$  is total spin on RE ion. The summation  $N$  runs over all possible set of neighbors. Considering exchange interaction between the nearest and next-nearest neighbor only we can write,  $\sum_{m=1}^N z_m J_m \approx (12J_1 + 6J_2)$ . Here the nearest neighbor exchange interaction  $J_1$  involves virtual excitation of majority 4f electron to the 5d band and subsequent exchange interaction with neighboring RE 4f spins. The next nearest neighbor superexchange interaction  $J_2$  is between two RE 5d bands mediated by N 2p band. Here  $J_1$  ( $J_1 > 0$ ) is ferromagnetic (FM) and  $J_2$  ( $J_2 < 0$ ) is antiferromagnetic (AFM) coupling. The exchange coupling constants  $J_{1,2}$  have shown to strongly depend on lattice constant and external magnetic field<sup>33,34</sup>. The AFM exchange  $J_2$  can lead to a component of the total moment on RE ions not aligned along net magnetization direction even below  $T_{Curie}$ <sup>35-37</sup>. Large external magnetic field can strengthen FM exchange  $J_1$  while weakening AFM exchange  $J_2$ . According to Eq. (3) this will lead to clear enhancement in  $T_{Curie}$ . Increase in  $T_{Curie}$  as shown in Fig. 1 strongly suggest suppression of AFM exchange with magnetic field. Large magnetic field can ease randomly unaligned moments line up along the net magnetization direction. This is similar to paramagnetism. Therefore, phenomenologically the field dependence of exchange splitting can be written as

$$E_{ex}(H) = E_{ex}(0) + E_{ex}^{sat} L(x), \quad (4)$$

where  $L(x) = \coth(x) - \frac{1}{x}$  is the Langevin function and  $x = \frac{\mu_{eff} H}{k_B T}$  is the ratio of magnetic energy to thermal energy. Here  $\mu_{eff}$  is the effective moment on RE ion pointing away from net magnetization direction<sup>38</sup>. The exchange splitting  $E_{ex}(0)$  and  $E_{ex}^{sat}$  denote zero field and saturation ( $H \rightarrow \infty$ ) value, respectively. In the limit  $x \ll 1$  (i.e,  $\mu_{eff} H \ll k_B T$ ), Eq. (4) can be written as

$$E_{ex}(H) = E_{ex}(0) + \alpha_s H, \quad (5)$$

where  $\alpha_s = \frac{\mu_{eff}}{3k_B T} E_{ex}^{sat}$ , is a temperature dependent constant. Exponential dependence of tunneling current on barrier height ensures that even a small change in  $E_{ex}(H)$  gets reflected in the tunneling conductance.

Magnetic property of Eu-chalcogenides and REN are analogues; in both the cases ferromagnetism originates from competing indirect exchange and superexchange interactions. In particular the electronic band structure in EuO and GdN are surprisingly similar. The only difference is the position of the 4*f* band in case of EuO is close to Fermi level above the anion 2*p* band. Therefore, the indirect exchange interactions in EuO is much stronger compared to GdN. Paramagnetic surface sheets are usually observed in EuO due to competing FM and AFM exchange coupling<sup>36</sup>. Magnetic field-enhanced spin-filtering has also been observed in EuSe which is considered to be an antiferromagnet at very low field and becomes ferromagnetic with large magnetic field<sup>39</sup>.

We now try to explain the magnetic field and bias current (voltage) dependence of the junction resistance using tunneling model. Similar to Mott's two-current model<sup>40</sup>, we assume the spin currents for spin-up and spin-down electrons are independent of each other. Therefore, the total conductance of our tunnel junction can be written as,  $G(V) = G_{\uparrow}(V) + G_{\downarrow}(V)$ , where  $G_{\uparrow}(V)$  and  $G_{\downarrow}(V)$  are conductances for up-spin and down-spin electrons, respectively. In the low voltage limit ( $V \rightarrow 0$ ) the conductances  $G_{\uparrow}(0)$  and  $G_{\downarrow}(0)$  can be calculated from Simmons' model<sup>24</sup> as:

$$G_{\uparrow(\downarrow)}(H) = \frac{3\sqrt{2m\Phi_{\uparrow(\downarrow)}}}{2d} \left(\frac{e}{\hbar}\right)^2 \exp\left(-\frac{2d}{\hbar} \sqrt{2m\Phi_{\uparrow(\downarrow)}}\right), \quad (6)$$

where  $m$  is mass of the electron,  $\hbar$  is the Planck's constant and  $d$  is the barrier width. For simplicity of calculation following Eq. (5), the barrier height for spin-up and spin-down electrons in presence of magnetic field can be written as;  $\Phi_{\uparrow} = \Phi_0 - E_{ex}(0) - \alpha_s H$  and  $\Phi_{\downarrow} = \Phi_0 + E_{ex}(0) + \alpha_s H$ , respectively. Calculated normalized junction resistance  $R_N(H) = \frac{G(0)}{G(H)}$ , for the DyN tunnel junction using Eq. (6) with  $\Phi_0 = 60$  meV and  $E_{ex}(0) = 5.6$  meV is shown in Fig. 6. Clearly one can see that as  $\alpha_s$  increases  $R_N(H)$  decrease rapidly and becomes nonlinear with magnetic field. The temperature dependence of  $R_N(H)$  shown in Fig. 3 is consistent with increase in  $\alpha_s$  with decreasing temperature. Although, our model provides a qualitative picture, for more accurate estimation of  $R_N(H)$  one has to consider bias voltage dependence of  $G(V)$  and exact functional dependence of  $E_{ex}(H)$  with magnetic field  $H$ . In our model, we have considered only direct tunneling process, however, other charge transport mechanism like sequential tunneling and inelastic cotunneling through defects in the barrier can also contribute to  $R_N(H)$ . Spin-flip scattering processes due to such charge transport mechanism can lead to significant reduction in  $R_N(H)$  calculated from our ideal model. Smaller  $R_N(H)$  for higher bias current as shown in Fig. 4 suggests possibility of a magneto-

electric coupling within the barrier. The magnetoelectric coupling can arise in our tunnel junctions due to double Schottky nature of these barriers. Earlier we have observed an electric field dependent spin-filter efficiency in NbN-GdN-NbN tunnel junctions<sup>20</sup>.

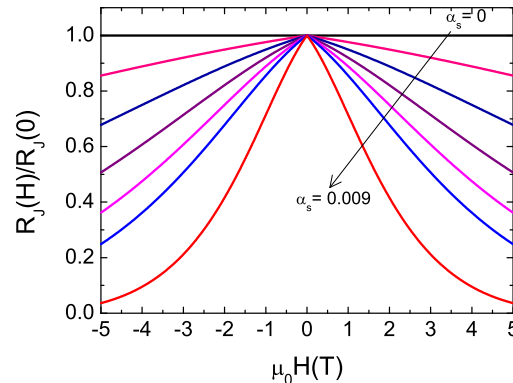


FIG. 6: (Color online) Calculated normalized junction resistance  $R_N(H)$  as a function of magnetic field for  $\alpha_s = 0$  to 0.009 (see text for details).

## V. CONCLUSIONS

In conclusion, we have fabricated spin-filter tunnel junctions with DyN and GdN tunnel barrier sandwiched between two superconducting NbN electrodes. We have made an extensive study on the effect of applied bias current and magnetic field on the spin-filtering efficiency. Using the Simmons model we have calculated barrier height  $\Phi_0 \approx 60$  and 111 meV for tunnel junction with DyN and GdN barriers, respectively. In DyN tunnel junctions, a small exchange splitting  $E_{ex}(0) \approx 5.6$  meV of the barrier height at 11 K resulted in  $\sim 37\%$  spin-filter efficiency. Larger  $E_{ex}(0) \approx 46$  meV lead to a huge  $\sim 97\%$  spin-filter efficiency in the case of GdN junctions. In DyN junctions the spin filter efficiency is found to increase to  $\sim 87\%$  when magnetic field  $H = 5$  T was applied. Similar field-induced increase in spin-filter efficiency was also found for GdN junctions. The increase in spin-filter efficiency can be understood by considering further lowering of the up-spin barrier height by magnetic field-induced increase in  $E_{ex}(H)$ . Magnetic field-induced enhanced ferromagnetism in these junctions were supported by observation of rise in  $T_{Curie}$  with magnetic field in  $R(T)$  measurements. Our findings are potentially useful for the control of spin polarized super-current in spintronics devices

## Acknowledgments

This work was supported by the ERC Advanced Investigator Grant SUPERSPIN. XLW acknowledges funding from the NSFC (Grant No. 11404323).



- 
- \* Electronic address: pkm27@cam.ac.uk
- <sup>1</sup> G.-X. Miao, M. Münzenberg, and J. S. Moodera, Rep. Prog. Phys. **74**, 036501 (2011).
  - <sup>2</sup> J. S. Moodera, T. S. Santos, and T. Nagahama, J. Phys.: Condens. Matter **19**, 165202 (2007).
  - <sup>3</sup> G. Schmidt, D. Ferrand, L. W. Molenkamp, A. T. Filip, and B. J. van Wees, Phys. Rev. B **62**, R4790 (2000).
  - <sup>4</sup> J. S. Moodera, X. Hao, G. A. Gibson, and R. Meservey, Phys. Rev. Lett. **61**, 637 (1988).
  - <sup>5</sup> X. Hao, J. S. Moodera, R. Meservey, Phys. Rev. B **42**, 8235 (1990).
  - <sup>6</sup> J. S. Moodera, R. Meservey, and X. Hao, Phys. Rev. Lett. **70**, 853 (1993).
  - <sup>7</sup> T. S. Santos and J. S. Moodera, Phys. Rev. B **69**, 241203(R) (2004).
  - <sup>8</sup> M. G. Chapline and S. X. Wang, Phys. Rev. B **74**, 014418 (2006).
  - <sup>9</sup> A. V. Ramos, M. J. Guittet, J. B. Moussy, R. Mattana, C. Deranlot, F. Petroff, and C. Gatel, Appl. Phys. Lett. **91**, 122107 (2007).
  - <sup>10</sup> U. Luders, M. Bibes, K. Bouzehouane, E. Jacquet, J.-P. Contour, S. Fusil, J.-F. Bobo, J. Fontcuberta, A. Barthélémy, and A. Fert, Appl. Phys. Lett. **88**, 082505 (2006).
  - <sup>11</sup> M. Gajek, M. Bibes, A. Barthélémy, K. Bouzehouane, S. Fusil, M. Varela, J. Fontcuberta, and A. Fert, Phys. Rev. B **72**, 020406(R) (2005).
  - <sup>12</sup> B. B. Nelson-Cheeseman, R. V. Chopdekar, L. M. B. Allredge, J. S. Bettinger, E. Arenholz, and Y. Suzuki, Phys. Rev. B **76**, 220410(R) (2007).
  - <sup>13</sup> R. V. Chopdekar, B. B. Nelson-Cheeseman, M. Liberati, E. Arenholz, and Y. Suzuki, Phys. Rev. B **83**, 224426 (2011).
  - <sup>14</sup> B. Prasad, M. Egilmez, F. Schoofs, T. Fix, M. E. Vickers, Wenrui Zhang, Jie Jian, Haiyan Wang, and Mark G. Blamire Nano Letters **14**, 2789 (2014).
  - <sup>15</sup> F. Natali, B. J. Ruck, N. O. V. Plank, and H. J. Trodahl, S. Granville, C. Meyer and W. R. L. Lambrecht, Progress in Materials Science **58**, 1316 (2013).
  - <sup>16</sup> C. G. Duan, R. F. Sabirianov, W. N. Mei, P. A. Dowben, S. S. Jaswal, and E. Y. Tsymbal, J. Phys.: Condens. Matter **19**, 315220 (2007).
  - <sup>17</sup> C. Meyer, B. J. Ruck, J. Zhong, S. Granville, A. R. H. Preston, G. V. M. Williams, and H. J. Trodahl, Phys. Rev. B **78**, 174406 (2008).
  - <sup>18</sup> K. Senapati, M. G. Blamire, and Z. H. Barber, Nature Materials **10**, 849 (2011).
  - <sup>19</sup> M. G. Blamire, A. Pal, Z. H. Barber, and K. Senapati, Proc. SPIE **8461**, 84610J (2012).
  - <sup>20</sup> A. Pal, K. Senapati, Z. H. Barber, M. G. Blamire, Adv. Mater. **25**, 5581 (2013).
  - <sup>21</sup> P. K. Muduli, A. Pal, M. G. Blamire, Phys. Rev. B **89**, 094414 (2014).
  - <sup>22</sup> P. Larson, W. R. L. Lambrecht, A. Chantis, and M. van Schilfgaarde, Phys. Rev. B **75**, 045114 (2007).
  - <sup>23</sup> M. Azeem, B. J. Ruck, Binh Do Le, H. Warring, H. J. Trodahl, N. M. Strickland, A. Koo, V. Goian and S. Kamba, J. Appl. Phys. **113**, 203509 (2013).
  - <sup>24</sup> J. G. Simmons, J. Appl. Phys. **34**, 1793 (1963).
  - <sup>25</sup> See supplementary material for fitting of I-V curve to Simmons model. The I-V and  $dI/dV - V$  of the junction measured at 4.2 K is also shown. Clear superconducting gap structure can be seen. This confirms electrical transport in our junctions is tunneling type.
  - <sup>26</sup> H. J. Trodahl, A. R. H. Preston, J. Zhong, B. J. Ruck, N. M. Strickland, C. Mitra, and W. R. L. Lambrecht, Phys. Rev. B **76**, 085211 (2007).
  - <sup>27</sup> C. Mitra and W. R. L. Lambrecht, Phys. Rev. B **78**, 195203 (2008).
  - <sup>28</sup> A. G. Petukhov, W. R. L. Lambrecht, and B. Segall, Phys. Rev. B **53**, 4324 (1996).
  - <sup>29</sup> Akira Hasegawa and Akira Yanase, J. Phys. Soc. Jpn. **42**, 492 (1977).
  - <sup>30</sup> A. Sharma and W. Nolting, Phys. Rev. B **81**, 125303 (2010).
  - <sup>31</sup> P. Liu, J. A. Colón Santana, Q. Dai, X. Wang, P. A. Dowben, and J. Tang, Phys. Rev. B **86**, 224408 (2012).
  - <sup>32</sup> J. Samuel Smart, *Effective Field Theories of Magnetism*, Saunders, (1966), Page 64.
  - <sup>33</sup> F. Leuenberger, A. Parge, W. Felsch, K. Fauth, and M. Hessler, Phys. Rev. B **72**, 014427 (2005); F. Leuenberger, A. Parge, W. Felsch, F. Baudelet, C. Giorgetti, E. Dartyge, and F. Wilhelm, Phys. Rev. B **73**, 214430 (2006).
  - <sup>34</sup> C. G. Duan, R. F. Sabirianov, Jianjun Liu, W. N. Mei, P. A. Dowben, and J. R. Hardy, Phys. Rev. Lett. **94**, 237201 (2005); C. G. Duan, R. F. Sabirianov, W. N. Mei, S. S. Jaswal, P. A. Dowben and E. Y. Tsymbal, Appl. Phys. Lett. **88**, 182505 (2006).
  - <sup>35</sup> K. Senapati, T. Fix, M. E. Vickers, M. G. Blamire and Z. H. Barber, J. Phys.: Condens. Matter **22**, 302003 (2010).
  - <sup>36</sup> K. Sattler and H. C. Siegmann, Phys. Rev. Lett. **29**, 1565 (1972).
  - <sup>37</sup> C. Demangeat and D. L. Mills, Phys. Rev. B **14**, 4997 (1976).
  - <sup>38</sup> The effective moment  $\mu_{eff}$  is much smaller than the total moment on RE ion;  $\mu = g\mu_B S$ . Only a small component of total moment on RE ion can point against net magnetization direction below  $T_{Curie}$  due to AFM exchange interaction. Here  $g$  is Landé g-factor and  $S$  is total spin on RE ion.
  - <sup>39</sup> J. S. Moodera, R. Meservey, and X. Hao, Phys. Rev. Lett. **70**, 853 (1993).
  - <sup>40</sup> N. F. Mott, Proc. Roy. Soc. A 153:699 (1936). N. F. Mott, Adv. Phys. **13**, 325 (1964).

### Supplementary Information

I-V measurements of our tunnel junctions were done at different temperatures. Tunnel barrier height was obtained by fitting IV curve to the Simmons model. For a rectangular barrier in the voltage range  $0 < V < \Phi_0$ , Simmons model expressed in practical units can be written as;

$$J(V) = \frac{6.2 \times 10^{10}}{d^2} \left[ \left( \Phi_0 - \frac{V}{2} \right) \exp(-1.025d \left( \Phi_0 - \frac{V}{2} \right)^{1/2}) - \left( \Phi_0 + \frac{V}{2} \right) \exp(-1.025d \left( \Phi_0 + \frac{V}{2} \right)^{1/2}) \right] \quad (7)$$

Here  $J(V)$  is expressed in  $\text{A}/\text{cm}^2$ ,  $\Phi_0$  in V and  $d$  in Å unit. Fig. 7 and 8 shows Simmons model fitting to IV curve measured above the Curie temperature  $T_{Curie}$  for the NbN - DyN(3 nm)- NbN and NbN-GdN(2.6 nm)-NbN tunnel junction, respectively.

We also measured I-V and  $dI/dV - V$  of the tunnel junctions below the critical temperature  $T_C$  of NbN. Fig. 9 and Fig. 10 shows normalized conductance spectra and I-V of the same junctions measured at 4.2 K. Superconducting gap structure with  $2\Delta \approx 2.88$  meV can be seen.

The I-V measurement shown in Fig.8 and Fig. 9 clearly imply that the electrical transport in our device is tunneling type.

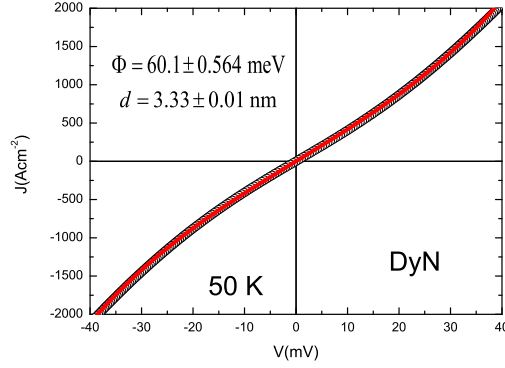


FIG. 7: (Color online) IV-curve measured at 50 K for the NbN - DyN(3 nm)- NbN tunnel junction. Solid red line shows fitting to the Simmons model.

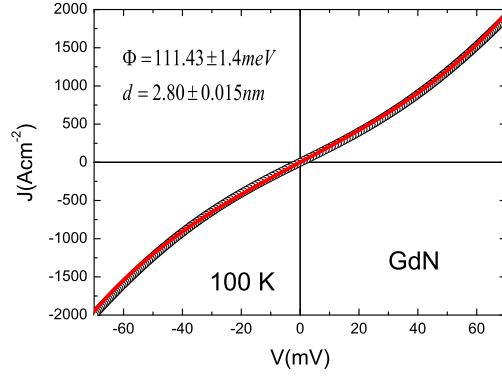


FIG. 8: (Color online) IV-curve measured at 100 K for the NbN-GdN(2.6 nm)-NbN tunnel junction. Solid red line shows fitting to the Simmons model.

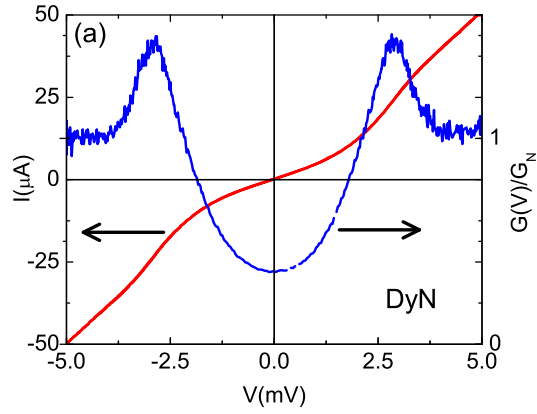


FIG. 9: (Color online) Normalized conductivity  $G(V) - V$  and I-V curve measured at 4.2 K for the NbN - DyN(3 nm)- NbN tunnel junction

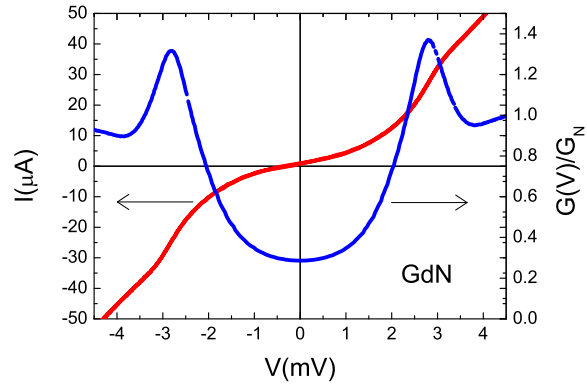


FIG. 10: (Color online) Normalized conductivity  $G(V) - V$  and I-V curve measured at 4.2 K for the NbN-GdN(2.6 nm)-NbN tunnel junction



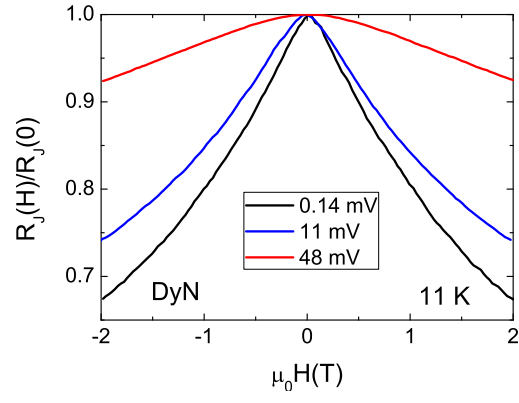


FIG. 11: (Color online) Magnetic field dependence of normalized junction resistance of the NbN - DyN(3 nm)- NbN tunnel junction measured with different bias voltage in constant voltage mode.